Crucial formula for determination of the occurrence of the nonchaotic states in rf-biased nonlinear oscillators

Tsung Hsun Yang
Institute of Electro-Optical Engineering, National Chiao-Tung University, 1001 Ta-Hsueh Road, Hsinchu, Taiwan 300, Republic of China

Ching Sheu Wang
Telecommunication Laboratories, Ministry of Transportation and Communications, Taoyuan, Taiwan 300, Republic of China

Jeun Chyuan Huang
Communication Technology Division, Industrial Technology Research Institute, Chung Chen Road, Hsinchu, Taiwan 300, Republic of China

Yih Shun Gou
Institute of Electrophysics, National Chiao-Tung University, 1001 Ta-Hsueh Road, Hsinchu, Taiwan 300, Republic of China
(Received 16 September 1994)

Crucial formulas to determine the nonchaotic states in rf-biased nonlinear oscillators are derived from numerical experiments. The nature of these formulas, which depends on symmetrical properties of the potential well, is investigated in terms of the driven frequency as a function of the damping constant κ. These formulas provide crucial guideposts to check which kinds of solutions (simple or complicated) can be tailored in the dissipative rf-biased nonlinear oscillators.

PACS number(s): 05.45.+b, 47.52.+j, 64.60.Cn, 64.10.+h

I. INTRODUCTION

In nonlinear oscillating systems with an external driving force, the equation of motion can be expressed in a general form,

$$\ddot{x}+\kappa\dot{x}+f(x)=F\sin\omega t\ , \tag{1}$$

where κ denotes the damping constant, F and ω represent the amplitude and frequency of the external periodic driving force, respectively, and $f(x)$ is the nonlinear term. If $f(x)$ is expressed as $x+x^2+\cdots$, Eq. (1) represents the dynamic motion of Duffing oscillators, whereas if $f(x)=\sin x$, the equation is called the resistively shunted Josephson junction model. Following previous work [1–8], the complicated solutions to Eq. (1), including period-2^k, chaotic, period-3×2^k, and period-$m\times 2^k$ solutions (k is a positive integer and m a prime number), have been formed in the parameter region where ω and κ are rather small. Moreover, the nonchaotic solutions to Eq. (1), including symmetric and asymmetric period-1 solutions, dominate in a region of large κ and large ω. In this case, regardless of the value of F, only symmetry-breaking bifurcations are observed.

In fact, an occurrence of nonchaotic states was first noted by McDonald and Plischke [9] in their study of the resistively shunted Josephson junction (RSJ) model [10,11] with the following criterion:

$$1\ll\kappa^2\ , \tag{2}$$

i.e., the damping constant is much larger than a unit. Subsequently, Kautz and Monaco [12,13] pointed out that chaos does not occur for

$$\omega\gg\kappa\ . \tag{3}$$

According to their suggestions, only simple or stable states can survive in some confined region of the parameter space of the higher damping and/or the faster driving frequency cases. Although these criteria can simplify the parameter regions of the complicated motion qualitatively, a quantitative resolution of this problem needs to be explored. In other words, the results described above immediately raise an intriguing question: can one predict quantitatively where or how a nonlinear oscillating system will display nonchaotic states in terms of chosen parameters ω and κ.

To this end, we will attempt to deduce certain crucial formulas in terms of the parameters, ω and κ with which one may quantitatively distinguish the existence of chaos from the occurrence of nonchaotic states in Eq. (1), not only in the RSJ model but also in Duffing oscillators. In what follows, we describe, with the aid of phase diagrams, bifurcation diagrams, state diagrams, and so on, the method used to derive the formulas. As compared with the RSJ model and the generalized Duffing oscillators, the physical implications of the symmetrical properties of potential wells with respect to the character of the formulas will be examined. Concluding remarks will be reported as well.

II. THE NUMERICAL SIMULATION

In order to derive the crucial formulas needed to distinguish the existence of chaos from the occurrence of

nonchaotic states in the more general cases of the dissipative nonlinear oscillator, two typical nonlinear oscillating systems, the RSJ model and Duffing oscillators, are considered here. All the variables and parameters used in this work are rescaled as dimensionless by means of some transformations [21,26] in order to directly compare the nature of the dynamics. In the numerical simulation, the fourth order Runge-Kutta algorithm [14] is employed to perform integration. Based on the integration, the Newton-Raphson method [14] is used to locate the stable and unstable fixed points on the Poincaré sections. Two scanning procedures, varying driving frequency at a fixed driving amplitude (ω scanning) and varying driving amplitude at a fixed driving frequency (F scanning), are employed with damping constant κ as a fixed parameter to extract as much information as possible. Consequently, various characteristics of all the thresholds of possible transitions in terms of the controlled parameters can be obtained and depicted in a state diagram.

In each state diagram of the respective systems, for example that shown in Fig. 1, there may exist a threshold frequency ω_T, at a fixed damping constant κ. We found that if the driving frequency is larger than the frequency ω_T in this damping case, no matter how large the driving force amplitude is, the chaotic solutions cannot exist. Then, by varying the damping constant κ to the other fixed value, we can obtain another ω_T via the same process. Finally, by repeating the process again and again, the relationship between ω_T and κ can be established. These relationships allow us to derive a boundary, and then to formulate a closed mathematical form in the ω-κ space by which the complicated solution region can be differentiated from the simple stable period-1 solution region. The details of these ω-κ relationships for the formulas for the RSJ model and the Duffing oscillators will be discussed below.

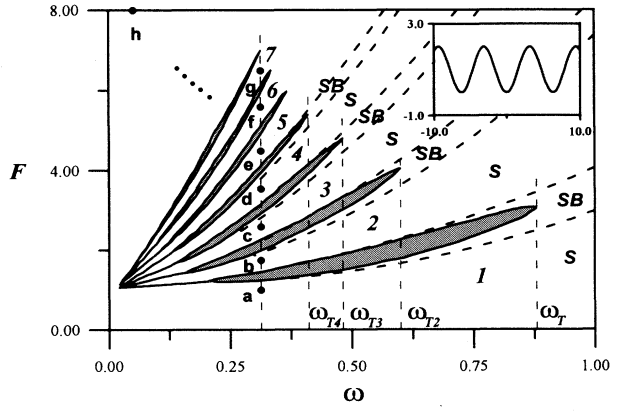

FIG. 1. State diagram of the RSJ model with $\kappa=1.0$. The shaded area denotes the complicated behavior regions including those caused by various kinds of bifurcations. There are no chaotic behaviors found if the rf frequency exceeds ω_T. The inset shows the corresponding potential well, $1-\cos X$. The integers from 1 to 7 reveal the corresponding number of local wells of the infinite sinusoidal potential within which the oscillating motion of the simple solution takes place. The phase portraits of the states marked $a-h$ are presented in Fig. 3. The symbols S and SB represents the symmetrical and symmetry-broken solutions, respectively.

A. RSJ model

The rf-biased RSJ model is given as

$$\ddot{x}+\kappa\dot{x}+\sin x=F\sin\omega t\ , \tag{4}$$

where κ is the damping constant, F is the amplitude of the rf driving force, and ω is the frequency of the rf driving force. Equation (4) describes the equation of motion of the phase difference of the junction. The equation can also be visualized as the dynamic motion of the swept angle of pendulum [9,10,15], the charge density wave [9], parametric amplifiers [16,17], etc. By means of the numerical method described above, the features of the state diagram with respect to various solutions of the states [9–21] in Eq. (4) will be presented. For the sake of illustration, only seven branches (shaded regions) are denoted in the F-ω state diagram where $\kappa=1.0$, as shown in Fig. 1. There are two kinds of solution regions. One contains the simple solution, including the period-1 oscillatory (symmetric and symmetry-broken) and the phase-locked traveling solutions. The other contains the complicated solution, including period-2^k, chaotic, period-3×2^k, period-$m\times2^k$ (k is a positive integer and m a prime), and the phase-unlocked traveling solutions. The shaded regions of the branches indicate the existence of the complicated solutions. Outside these regions, especially in the region where the frequency is above ω_T, the simple solutions exist without the chaotic ones. In fact, the scenario of a sequence of bifurcations along the F axis at a fixed frequency ω is nearly the same in each branch, as shown in Fig. 2. They mainly contain period-doubling

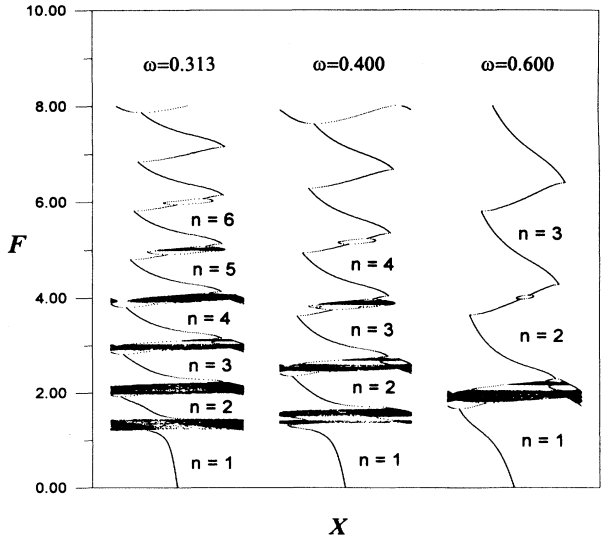

FIG. 2. Three bifurcation diagrams of the RSJ model with $\omega=0.313$, 0.400, and 0.600, $\kappa=1.0$, $F=0.0$–8.0. All the responses on the Poincaré sectin are carried in the intervals of $[-\pi,\pi]$ by the transform of $X\pm2m\pi$. Similar scenarios of bifurcations appear again and again in each branch n.

cascades, chaos, intermittency, crisis, and reverse period-doubling cascades. The period-3 windows and sometimes the period-5 windows very often burst out within the chaotic events. Since similar scenarios of bifurcation appear again and again in each branch, it clearly implies self-similarity of the solutions embedded in the RSJ model. Such self-similar properties will be shown in greater detail below.

As is also shown in Fig. 1, the territory of the each branch is bounded by the terrain of the symmetry-breaking (SB) solution. Also, the regions of the symmetric solution exist between the regions of the SB solutions. Moreover, the frequency of both the symmetric and the SB solutions is period-1. The shaded regions of the branches will shrink and finally merge as ω is decreased and F is increased further and further. We find that in the upper left-hand corner of Fig. 1 many more branches still exist.

In addition to the evidence of the above observations, the self-similar feature of the bifurcation in each branch in the RSJ model can be further illuminated as follows. First, as shown in Fig. 1, the terrain of each simple solution separated by the branches of the complicated regions is indicated by a series of consecutive integers. We note that the integers reveal the corresponding number of local wells of the infinite sinusoidal potential within which the oscillating motion of the simple solution is executed in the RSJ model. For example, in the case of $\omega=0.313$, $F=1.20$, and $\kappa=1.0$, the response is an oscillating motion in the $n=2$ regime, as shown in Fig. 1, and corresponds to the swinging between two local wells of the sinusoidal potential within the interval of one period of the rf biasing, as shown in Fig. 3(b). Similarly, the phase portraits, as shown in Figs. 3(a)–3(g), illustrate these behaviors from $n=1$ to $n=7$, respectively, when F increases from 1.80 to 7.0 for $\omega=0.313$. The situation is further illustrated in Fig. 3(h) for $n=51$. In the complicated region, the common response of swinging from the nth local well to the $n+1$th results from two stable solutions merging with an unstable one located on top of the sinusoidal well. In other words, the respective asymmetrical solutions in the adjacent wells are merging into one solution. This leads to the swinging to the next well after the collision between the asymmetrical solutions and the

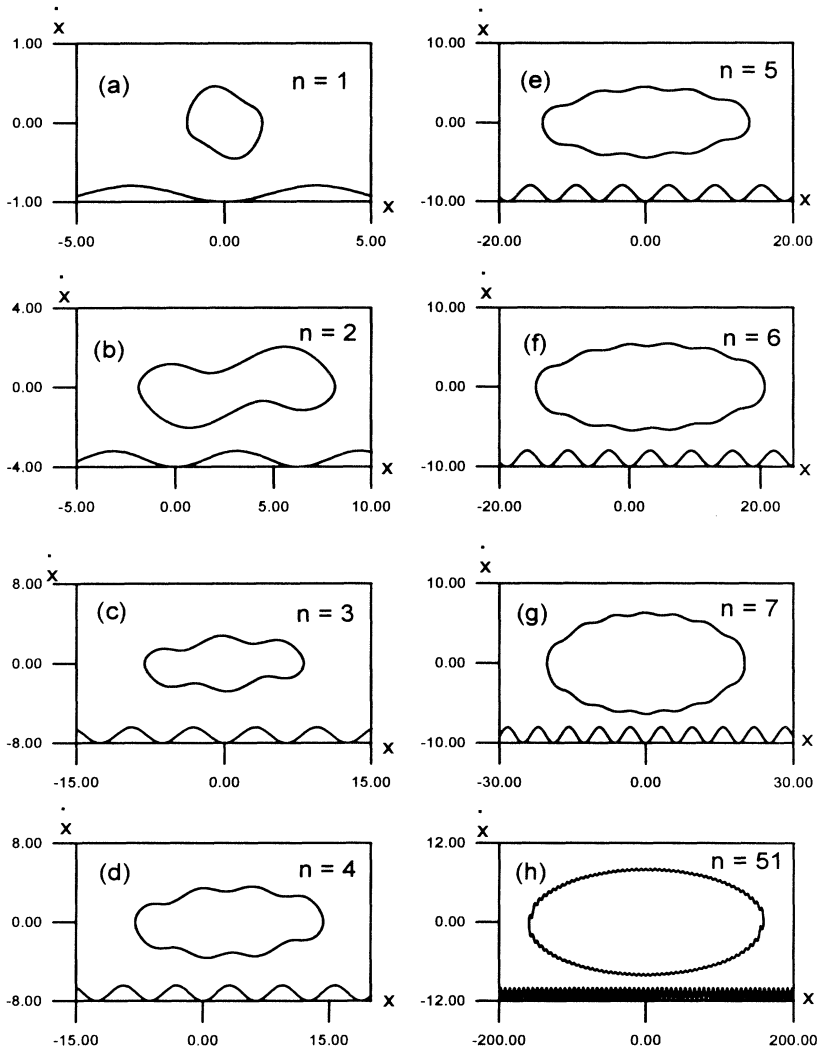

FIG. 3. Phase portraits with $\kappa=1.0$, $\omega=0.313$, and (a) $F=1.00$, $n=1$; (b) $F=1.75$, $n=2$; (c) $F=2.60$, $n=3$; (d) $F=3.55$, $n=4$; (e) $F=4.50$, $n=5$; (f) $F=5.60$, $n=6$; (g) $F=6.50$, $n=7$; (h) $\omega=0.05$, $F=8.00$, $n=51$. The value of n represents the corresponding number of local wells of the infinite sinusoidal potential within which the oscillating motion of the simple solution takes place.

unstable.

It is also worth noting that all the branches in the state diagram at a fixed damping constant κ are located within the region where the driving frequency is less than the critical threshold frequency ω_T. If the driving frequency is larger than the critical threshold frequency ω_T, no matter how large the driving force amplitude is, the complicated solutions cannot exist. As mentioned before, for a fixed damping constant κ, we obtain a threshold frequency ω_T. Consequently, we find quantitatively that the critical threshold frequency ω_T at the first branch, $n=1$, is dependent on the damping constant κ. This is shown with a simple relation,

$$\omega_T=\omega_0\left[1-\left[\frac{\kappa}{\kappa_0}\right]^2\right], \tag{5}$$

where $\omega_0=1.450$ and $\kappa_0=1.681$. Figure 4(a) shows the relation between the critical threshold frequency ω_T and damping constant κ (both the numerical data and the fitting function). It clearly shows the boundaries differentiating the regions of the complicated solutions and those of the simple ones. According to this relation, it is apparent that chaos occurs not only in the overdamped case, $\kappa\gg1$, but also in the underdamped case $\omega\gg\kappa$. Although these results have been qualitatively suggested by McDonald and Plischke, and by Kautz previously, we can quantitatively predict here from Eq. (5) that if the damping constant κ exceeds a threshold value of κ_0, then no chaotic behavior can be found. Therefore, we emphasize that Eq. (5) provides valuable information for determining quantitatively the nonchaotic states in the RSJ model.

Using the self-similar feature mentioned above, we further conjecture that each maximum driving threshold frequency of the nth branches, ω_{Tn}, depends on the damping constant κ, as does the critical threshold frequency ω_T (for the branch $n=1$). From Eq. (5), we surmise that it might be scaled as follows:

$$\omega_{Tn}=\omega_T n^{-\delta}=\omega_0\left[1-\left[\frac{\kappa}{\kappa_0}\right]^2\right]n^{-\delta}, \tag{6}$$

where the parameter δ depends on the damping constant κ. In what follows, the equation will be verified tentatively in order to make it appear plausible.

First, the respective threshold frequencies of the nth branches, ω_{Tn}, are traced out under one fixed damping constant κ by the driving amplitude scanning method (F scanning). Then, changing the damping constant κ to a different value, a new set of threshold frequencies ω_{Tn} can also be found in the same fashion. After collecting

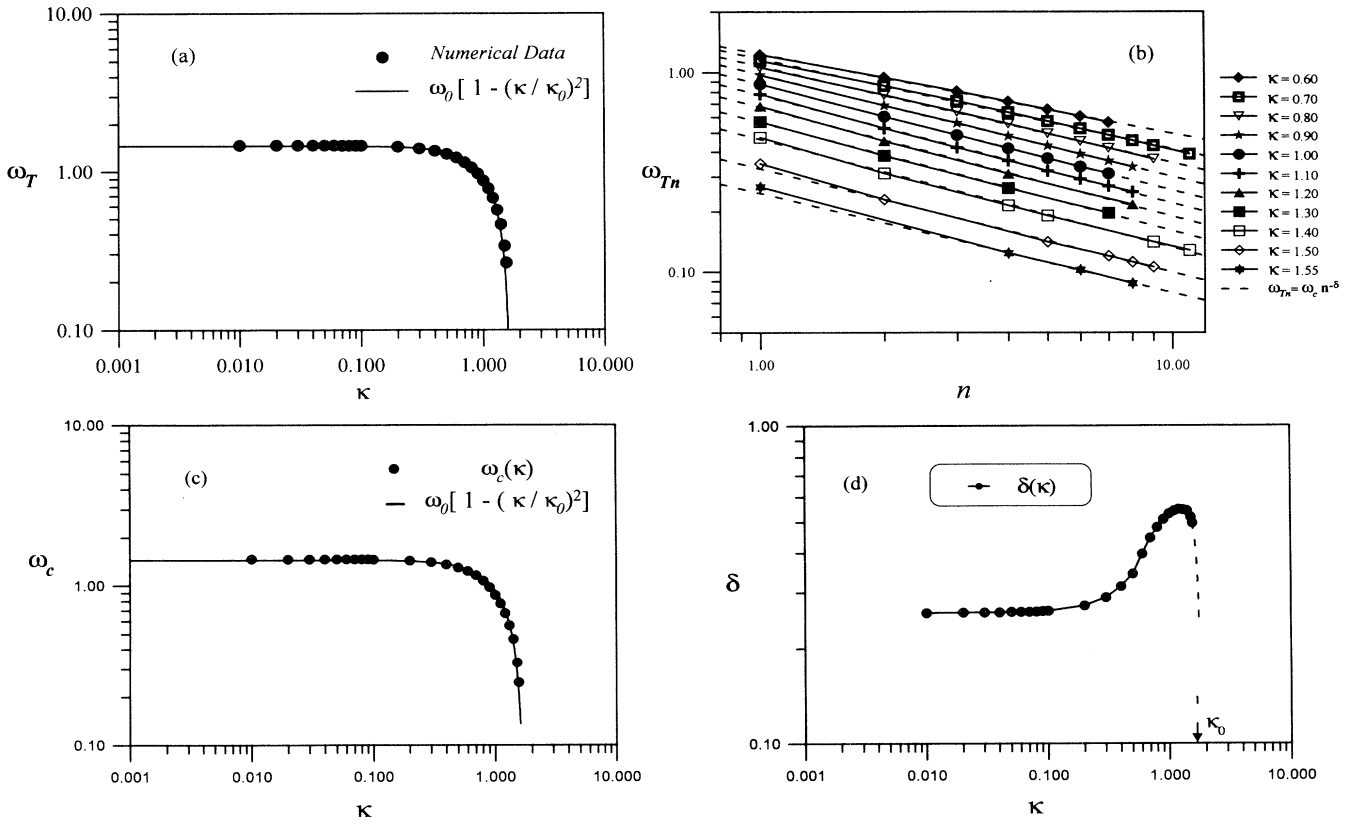

FIG. 4. (a) Numerical simulation data (●) of ω_T-κ compared with the fitting function (–) $\omega_T=\omega_0[1-(\kappa/\kappa_0)^2]$, where $\omega_0=1.450$ and $\kappa_0=1.681$. (b) Numerical simulation data ω_{Tn}-n for various values of κ and fitted by the functional relation $\omega_{Tn}=\omega_c n^{-\delta}$. (c) Dependence on κ of fitting constant ω_c (●) obtained from Fig. 4(b). (d) Dependence on κ of fitting constant δ obtained from Fig. 4(b).

all of the ω_{Tn}-n relations that depend on various values of the damping constant κ, we summarize them in Fig. 4(b). In the log-log coordinate, we find the linear relation between the logarithm of the threshold frequency ω_{Tn} and the branch number n. The properties of ω_{Tn} and n enable us to determine their functional equation,

$$\omega_{Tn}=\omega_c(\kappa)n^{-\delta(\kappa)} , \tag{7}$$

where the function $\omega_c(\kappa)$ is dependent on the damping constant κ and the exponent δ is the slope of the straight lines in Fig. 4(b) for the corresponding damping constant κ. Note that such a simple power law relation apparently reveals the nature of renormalization, i.e., it reproduces itself upon rescaling.

In order to verify Eq. (6), we still need to examine the properties of $\omega_c(\kappa)$ in greater detail. This immediately raises the question of whether or not the function $\omega_c(\kappa)$ for arbitrary n can be taken as the functional form $\omega_T=\omega_0[1-(\kappa/\kappa_0)^2]$ for $n=1$ in Eq. (6). We resolve this in Fig. 4(c). The figure clearly shows that the property of the function ω_c is consistent with that of the functional form $\omega_T=\omega_0[1-(\kappa/\kappa_0)^2]$. Note that the exactness of Eq. (6) is entirely a consequence of the emergence in the RSJ model of the self-similar feature under the nonlinear dynamics.

Following the spirit of the physical implication of the renormalization method, we attempt to explore the features of the exponent δ. Since the value of the exponent δ depends on the damping constant κ [as in Fig. 4(d)], we present three different cases. For the case of the small damping constant κ ($\lesssim 0.1$), the exponent δ reaches a constant (≈ 2.589) and is nearly independent of the damping constant κ. In the case where the damping constant κ gets larger and larger ($\gtrsim 0.5$), the increasing of exponent δ behaves in hypertangent form and then reaches its maximum. Finally, right after the damping constant reaches maximum, the exponent δ drops rapidly to zero as the value of the damping constant κ approaches the threshold value of κ_0. All these results of the exponent δ can be utilized to quantitatively demonstrate the self-similar behavior.

B. Duffing oscillators

The generalized rf-biased Duffing oscillator governed by the equation is given as

$$\ddot{x}+k\dot{x}+\frac{dV(x)}{dx}=F\sin\omega t , \tag{8}$$

where the overdot denotes the derivative with respect to time t, κ is the damping factor, and $V(x)$ is an anharmonic potential function. This equation has been utilized to model a wide variety of physical systems, such as optical bistability in the multiple-photon absorption process, soft and hard springs, buckled beam, four wave interaction, plasma oscillation [22–25], etc. In general, the potential function $V(x)$ is described by

$$V(x)=\frac{\alpha}{2}x^2+\frac{\beta}{3}x^3+\frac{\gamma}{4}x^4 , \tag{9}$$

with α, β, and γ coefficients. Actually, by means of some transformations [26], it embraces four fundamental types of potentials: $V_1=\frac{1}{2}x^2-\frac{1}{3}x^3$, $V_2=-\frac{1}{2}x^2+\frac{1}{4}x^4$, $V_3=\frac{1}{2}x^2-\frac{1}{4}x^4$, and $V_4=\frac{1}{2}x^2+\frac{1}{4}x^4$. The features of the state diagrams of these four types are listed, as follows.

1. V_1 potential ($V_1=\frac{1}{2}x^2-\frac{1}{3}x^3$) [27,28]

The state diagram for this case is shown in Fig. 5(a). The transition boundaries include hysteresis, period doubling (PD), crisis, and intermittency. In this state diagram, we also note that the PD curve folds back at a frequency ω_T. The complicated solutions exist only with the parameters ω below the threshold value ω_T. According to our experiments, like that of the RSJ model, the threshold frequency ω_T is found to be a function of the damping constant κ through a simple form,

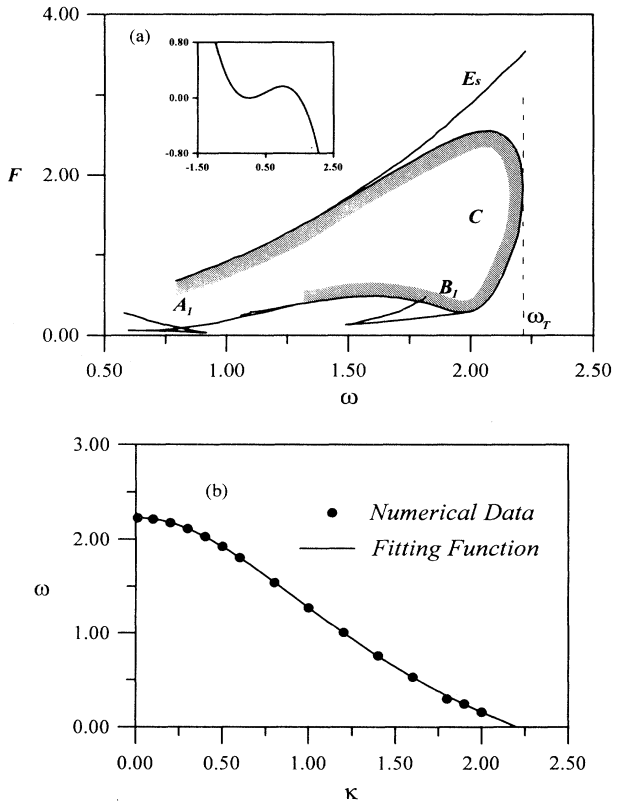

FIG. 5. (a) State diagram of the rf-biased asymmetrical one-well Duffing oscillator, including the primary (A_1) and subharmonic (B_1) resonance regions. C denotes the complicated solution region enclosed by period-doubling and reverse period-doubling transition boundaries, and Es denotes the escaping boundary. ω_T indicates the maximum rf frequency at which chaotic behaviors can exist. The potential well is drawn in the inset. (b) the $\omega_T-\kappa$ relation, $\omega_T(\kappa)=\omega_0[1+C_1(\kappa/\kappa_0)-C_2(\kappa/\kappa_0)^2+C_3(\kappa/\kappa_0)^3-C_4(\kappa/\kappa_0)^4]$ with $\omega_0=2.226$, $\kappa_0=2.220$, $C_1=0.101$, $C_2=4.011$, $C_3=4.495$, and $C_4=1.585$, of the rf-biased Duffing oscillator with asymmetrical one-well potential. The black dots denote the experimental simulation data and the solid line for fitting.

$$\omega_T(\kappa)=\omega_0\left[1+C_1\left[\frac{\kappa}{\kappa_0}\right]-C_2\left[\frac{\kappa}{\kappa_0}\right]^2+C_3\left[\frac{\kappa}{\kappa_0}\right]^3-C_4\left[\frac{\kappa}{\kappa_0}\right]^4\right], \quad (10)$$

where $\omega_0=2.226$, $\kappa_0=2.200$, $C_1=0.101$, $C_2=4.011$, $C_3=4.495$, and $C_4=1.585$ [see Fig. 5(b)]. κ_0 is required in order to satisfy $\omega_T(\kappa_0)=0$. Moreover, the nontrivial coefficients of odd order of (κ/κ_0), C_1, and C_3, are induced by the asymmetrical property of the potential well with respect to the origin, while they are equal to zero in the case of the symmetrical ones.

2. V_2 potential ($V_2=-\frac{1}{2}x^2+\frac{1}{4}x^4$) [29,30]

Figure 6(a) shows the state diagram for this case. The potential well V_2 has two local wells separated by a bump in the middle. Due to the motion in one of the local wells, the shape of the transition boundaries resembles a swallow's tail. The curves of period doubling are folded. The threshold frequency ω_T is found to be dependent on the damping constant κ, and this relation can be fitted to satisfy the following equations:

$$\omega_T(\kappa)=\omega_0\left[1-\left[\frac{\kappa}{\kappa_0}\right]^2\right], \quad (11)$$

where the constants $\omega_0=3.218$ and $\kappa_0=2.050$ [see Fig. 6(b)]. If the driving frequency is beyond the threshold frequency ω_T and the driving force amplitude does not exceed the boundary H_{up}, the complicated solution cannot occur. Equation (11) provides a crucial condition with which to determine whether the solution is simple or complicated. All these observed features in this system are the same as those of the RSJ model. With a further increase of the excitation amplitude up to curve H_{up}, the solution becomes stable with the swing through two valleys. In this situation, the dynamics of the swing closely

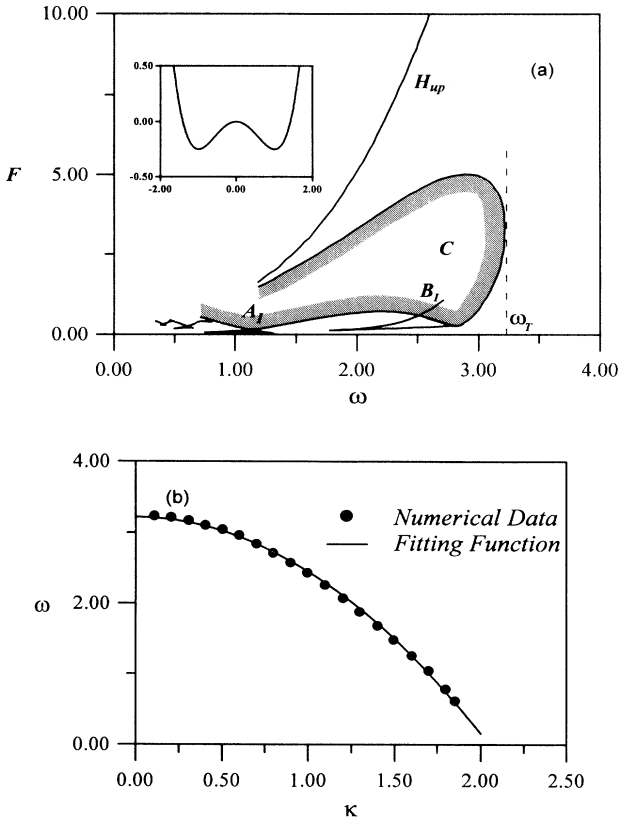

FIG. 6. (a) State diagram of the rf-biased symmetrical two-well Duffing oscillator including the primary (A_1) and subharmonic (B_1) resonance regions. C denotes the complicated solutions region enclosed by period-doubling and reverse period-doubling transition boundaries and H_{up} denotes the jump-up boundary. The potential well is shown in the inset. As long as the rf frequency is above ω_T and the rf amplitude is below the H_{up} transition boundary, there are no chaotic behaviors found. (b) ω_T-κ relation [Eq. (11)] $\omega_T=\omega_0[1-(\kappa/\kappa_0)^2]$, with $\omega_0=3.218$ and $\kappa_0=2.050$, of the rf-biased Duffing oscillator with symmetrical two-well potential.

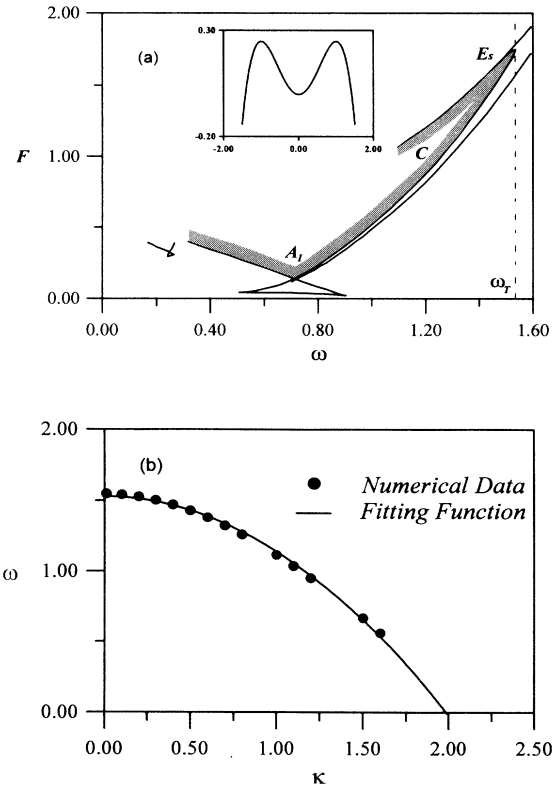

FIG. 7. (a) State diagram of the rf-biased symmetrical one-well Duffing oscillator. The primary resonance region is marked A_1. C denotes the complicated solution region enclosed by period-doubling and reverse period-doubling transition boundaries, and Es denotes the escaping boundary. The potential well is shown in the inset. As long as the rf frequency is above ω_T, no chaotic behaviors are found. (b) The ω_T-κ relation [Eq. (12)] $\omega_T=\omega_0[1-(\kappa/\kappa_0)^2]$, with $\omega_0=1.528$ and $\kappa_0=1.985$, of the rf-biased Duffing oscillator with symmetrical one-well potential.

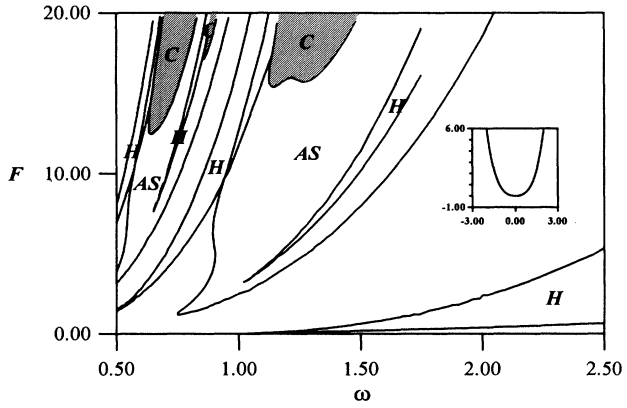

FIG. 8. State diagram of the Duffing oscillator with infinite potential well. The transition boundaries shown include saddle-node (H), symmetry-breaking (AS), and period-doubling and reverse period-doubling (C) bifurcation. The shaded areas denote the complicated solution regions. There is no ω_T found.

resembles the case of the infinitely bounded potential V_4, while the small effect of the bump in the well is negligible.

3. V_3 potential ($V_3=\frac{1}{2}x^2-\frac{1}{4}x^4$) [31]

The state diagram for the transition boundaries with the swallow-tailed form is shown in Fig. 7(a) with damping constant $\kappa=0.1$. The transitions include hysteresis, SB, PD, crisis, and intermittency. Because the potential barrier is finite, the response will be escape from the well after a sequence of bifurcations of Feigenbaum period doubling and/or intermittency routes to chaos. The threshold frequency ω_T at which the PD curve folds back is well fitted in terms of the damping constant κ, as shown in the following relation:

$$\omega_T(\kappa)=\omega_0\left[1-\left[\frac{\kappa}{\kappa_0}\right]^2\right], \tag{12}$$

where the constants $\omega_0=1.528$ and $\kappa_0=1.985$ [see Fig. 7(b)]. With a driving frequency higher than the threshold frequency ω_T, only the simple period-1 solutions are obtainable.

4. V_4 potential ($V_4=\frac{1}{2}x^2+\frac{1}{4}x^4$) [32–35]

The potential is symmetrical, without any inflection point, and is infinitely bounded as $|x|\rightarrow\infty$. The state diagram is shown in Fig. 8. The shapes of the transition boundaries are no longer swallow tailed and can be classified into two groups with characteristic shapes associated with odd and even resonances. The chaotic solutions exist in the even resonant regions (marked C in Fig. 8). No threshold frequency ω_T is observed. Also, there is no appearance of a similar ω_T-κ functional relation function in a closed form.

III. CONCLUSION

In this work, we have systematically examined the rf-biased Josephson junction and the Duffing oscillators in a wide range of parameter space. The crucial formulas of the functional relation, ω_T vs κ, have been derived to give clear-cut criteria for determining the existence of the nonchaotic states. Together with our preceding report [26], it is worth mentioning that the functional ω_T-κ relation can be obtained in those potentials that possess the inflection points only. Furthermore, for potential wells that are symmetrical with respect to the origin of the potential, the ω_T-κ relation is in the form $\omega_T=\omega_0[1-(\kappa/\kappa_0)^2]$, while for asymmetrical potential wells, the ω_T-κ relation is in the form $\omega_T(\kappa)=\omega_0[1+C_1(\kappa/\kappa_0)-C_2(\kappa/\kappa_0)^2+C_3(\kappa/\kappa_0)^3-C_4(\kappa/\kappa_0)^4]$. In addition, the embedded feature of the self-similarity in the RSJ model is also extended to obtain the power law relation between the threshold frequency of each branch, ω_{Tn}, and the branch number n. The threshold frequency of each branch, ω_{Tn}, is rescaled by the branch number n as $\omega_{Tn}=\omega_0[1-(\kappa/\kappa_0)^2]n^{-\delta}$. According to the conventional physical implication of the renormalization method, the exponent δ has been found to present different kinds of behaviors under three stages of the damping constant κ. On the basis of these formulas, a solution to the nonlinear oscillating system could be almost precisely expressed as $x=a\sin(\omega t+\phi)$ in a chaos-free region. In other words, these formulas provide crucial guideposts with which to check which kinds of solutions (simple or complicated) can be tailored in the dissipative rf-biased nonlinear oscillators.

ACKNOWLEDGMENT

This work was supported by the National Science Council of the Republic of China (Taiwan) under Contract No. NSC83-0208-M009-37.

[1] J. P. Eckmann, Rev. Mod. Phys. **53**, 643 (1981).
[2] E. Ott, Rev. Mod. Phys. **53**, 655 (1981).
[3] M. J. Feigenbaum, J. Stat. Phys. **19**, 25 (1978).
[4] P. Manneville and Y. Pomeau, Commun. Math. Phys. **74**, 189 (1980).
[5] D. Rulle and F. Takens, Commun. Math. Phys. **20**, 167 (1971).
[6] C. Grebogi, E. Ott, and J. A. Yorke, Physica **7D**, 181 (1983).
[7] J. Guckenheimer and P. Holmes, *Nonlinear Oscillator, Dynamical Systems, and Bifurcations of Vector Fields* (Springer-Verlag, New York, 1983).
[8] J. M. T. Thompson and H. B. Stewart, *Nonlinear Dynamics and Chaos: Geometrical Methods for Engineers and*

Scientists (Wiley, New York, 1987).
[9] A. H. MacDonald and M. Plischke, Phys. Rev. B **27**, 201 (1983).
[10] D. E. McCumber, J. Appl. Phys. **39**, 3113 (1968).
[11] W. C. Stewart, Appl. Phys. Lett. **12**, 277 (1968).
[12] R. L. Kautz, J. Appl. Phys. **52**, 6241 (1981).
[13] R. K. Kautz and R. Monaco, J. Appl. Phys. **57**, 875 (1985).
[14] T. S. Parker and L. O. Chua, *Practical Numerical Algorithms for Chaotic Systems* (Springer-Verlag, New York 1989).
[15] R.L. Kautz, IEEE Trans. Magn. **MAG-19**, 465 (1983).
[16] M. T. Levinsen, R. P. Chiao, M. F. Feldman, and B. A. Tucker, Appl. Phys. Lett. **31**, 776 (1976).
[17] R. L. Peterson and D. G. MacDonald, IEEE Trans. Magn. **MAG-13**, 887 (1977).
[18] B. A. Huberman, J. P. Crutchfield, and N. H. Packard, Appl. Phys. Lett. **37**, 750 (1980).
[19] D. D'Humieres, M. R. Beasley, B. A. Huberman, and A. Libchaber, Phys. Rev. A **26**, 3483 (1982).
[20] Y. H. Kao, J. C. Huang, and Y. S. Gou, J. Low Temp. Phys. **63**, 287 (1986).
[21] J. C. Huang, Ph.D. thesis, Institution of Electronics, National Chiao Tung University, Taiwan, 1989.
[22] B. Ritchie and C. M. Bowden, Phys. Rev. A **32**, 2293 (1985).
[23] B. A. Huberman and J. P. Crutchfield, Phys. Rev. Lett **43**, 1743 (1979).
[24] P. Holms, Philos. Trans. R. Soc. London, Ser. A **292**, 419 (1979).
[25] F. T. Arecchi and F. Lsi, Phys. Rev. Lett. **49**, 94 (1982).
[26] C. S. Wang, Y. H. Kao, J. C. Huang, and Y. S. Gou, Phys. Rev. A **45**, 3471 (1992).
[27] J. M. T. Thompson, Proc. R. Soc. London, Ser. A **421**, 195 (1989).
[28] J. C. Huang, Y. H. Kao, C. S. Wang, and Y. S. Gou, Phys. Lett. A **136**, 131 (1989).
[29] Y. H. Kao, J. H. Huang, and Y. S. Gou, Phys. Rev. A **35**, 5228 (1987).
[30] V. Englisch and W. Lauterborn, Phys. Rev. A **44**, 916 (1991).
[31] Y. H. Kao, J. H. Huang, and Y. S. Gou, Phys. Lett. A **131**, 91 (1988).
[32] Y. Ueda, J. Stat. Phys. **20**, 181 (1979).
[33] U. Parlitz and W. Lauterborn, Phys. Lett. **107A**, 351 (1985).
[34] Y. H. Kao, C. S. Wang, and T. H. Yang, J. Sound Vibration **159**, 13 (1992).
[35] U. Parlitz, Int. J. Bifurcation Chaos **3**, 703, (1993).